Theoretical Study on the Excited-State Intramolecular Proton Transfer in the Aromatic Schiff Base Salicylidene Methylamine: an Electronic Structure and Quantum Dynamical Approach

Juan Manuel Ortiz-Sánchez, Ricard Gelabert,* Miquel Moreno, and José M. Lluch

Departament de Química, Universitat Autònoma de Barcelona, 08193 Bellaterra, Barcelona, Spain

Received: January 23, 2006; In Final Form: February 23, 2006

The proton-transfer dynamics in the aromatic Schiff base salicylidene methylamine has been theoretically analyzed in the ground and first singlet (π,π^*) excited electronic states by density functional theory calculations and quantum wave-packet dynamics. The potential energies obtained through electronic calculations that use the time-dependent density functional theory formalism, which predict a barrierless excited-state intramolecular proton transfer, are fitted to a reduced three-dimensional potential energy surface. The time evolution in this surface is solved by means of the multiconfiguration time-dependent Hartree algorithm applied to solve the time-dependent Schrödinger equation. It is shown that the excited-state proton transfer occurs within 11 fs for hydrogen and 25 fs for deuterium, so that a large kinetic isotope effect is predicted. These results are compared to those of the only previous theoretical work published on this system [Zgierski, M. Z.; Grabowska, A. *J. Chem. Phys.* **2000**, *113*, 7845], reporting a configuration interaction singles barrier of 1.6 kcal mol^{-1} and time reactions of 30 and 115 fs for the hydrogen and deuterium transfers, respectively, evaluated with the semiclassical instanton approach.

1. Introduction

Photochromism in organic molecules[1−3] has been the target of many studies, both from the experimental and theoretical points of view.[4−7] Photochromism is well-known to be among the fastest chemical reactions occurring in nature, and includes processes such as cis−trans isomerization, photochemical ring-closure−ring-opening reactions, or excited-state intramolecular proton transfer (ESIPT).

A very special interest has been placed on aromatic molecules, and more concretely on the family of the aromatic Schiff bases.[8] These compounds comprise a wide range of structures, including one or two proton-transfer centers involving functional groups with opposite pK_a tendencies (e.g., OH and imine), which can lead to single or double ESIPT processes. This large variety of possible structures has attracted much attention over the past years, and examples such as salicylideneaniline (SA) or *N*,*N*′-bis(salicylidene)-*p*-phenylenediamine (BSP) have been thoroughly studied.[9−14] The structures of these molecules are depicted in Figure 1.

It is agreed that the photoexcitation of these compounds, which has mainly been characterized as a HOMO−LUMO ($\pi \rightarrow \pi^*$) transition, is followed by an ultrafast proton transfer along the intramolecular hydrogen bond of the *o*-hydroxyl group to the imine nitrogen to give the cis-keto tautomer within a few femtoseconds. The (π,π^*) singlet state of the cis-keto form undergoes subsequent isomerization to a trans-keto form as the final photoproduct. In addition, the excited cis-keto form can also return back again to the ground state by either a thermal or a photochemical process, completing the reversible cycle. The reversible nature of this process has great importance in technological applications in devices such as rewritable molecular memories and switches.[15−20] However, facts such as the existence of many isomeric structures and the possibility of conical intersections before and after the proton transfer make this mechanism still ambiguous and controversial, especially the depopulation processes following the ESIPT.

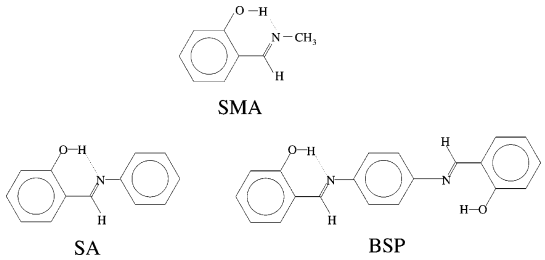

Figure 1. Structures of some relevant photochromic Schiff bases: SMA, SA, and BSP.

As a complement to the modern ultrafast experimental techniques such as time-resolved laser spectroscopy, which is very helpful in the study of photochromic processes,[21] theoretical studies are a powerful and valuable tool in the analysis of these processes. The availability of advanced theoretical methods allows one to deal with many-atom systems with good accuracy and reasonable cost. However, the necessity to begin with smaller systems in order to better understand the complexity of larger systems, for example, SA or BSP, is still present. The simplest aromatic Schiff base that presents photochromic properties is the salicylidene methylamine (SMA), also depicted in Figure 1.

Despite its simple molecular structure, very little has been published about the properties and behavior of SMA. The synthesis,[22] a study of the enol-keto equilibrium as a function of temperature in a protic solvent (methanol) performed by electronic absorption and Raman spectroscopy,[23] and complete spectral data on SMA involving the transient absorption spectra[24] have been reported. From the latter work, the absorption

* Corresponding author. E-mail: ricard.gelabert@uab.es.

10.1021/jp0604600 CCC: $33.50
Published on Web 03/23/2006

maximum energy of SMA has been measured to be around 32 000 cm^{-1}, which is, up to now (to our knowledge) one of the few direct experimental measurements we can compare our theoretical results to.

On the other hand, just one theoretical study, by Zgierski and Grabowska,[25] has been reported for SMA. In that work, an exploration of the ground and first singlet excited electronic states was performed at the HF/6-31G(d) and CIS/6-31G(d) levels of theory, respectively, in addition to some complementary calculations carried out with the TDDFT/B3LYP/6-31G(d) and semiempirical CNDO/S+CISD methods. According to their results, five energy minima corresponding to the enol, cis-keto, and three trans-keto tautomers were located. A small energy barrier for the ESIPT was calculated on the first singlet excited electronic state of 1.62 kcal mol^{-1}. Also, dynamical calculations were performed applying the semiclassic instanton approach,[26] with the use of the geometries and force field of the stationary points located in the first singlet excited state. Their results predicted that the proton-transfer reaction would take place within 30 fs for hydrogen and 115 fs for deuterium.

Nevertheless, it should be remembered that the configuration interaction singles (CIS) level tends to exaggerate the excitation and barrier energies for the ESIPT.[27,28] On the other hand, dynamical calculations with the energy origin placed in the energy minima rather than in the vertical excitation energies tend to increase the time scale of the processes. For these reasons, in the present work, we want to focus on the ESIPT reaction of SMA from the theoretical point of view, first applying more accurate quantum electronic methods to study the topology of the ground and first singlet excited electronic states, and then using these results to carry out quantum dynamical calculations, starting from the vertical excitation energies, to determine the time scale of proton transfer in the first singlet excited electronic state.

2. Computational Details

Two different sets of calculations were necessary to study the dynamics of the ESIPT in SMA. First, electronic-structure calculations have been used to explore the topology of the ground (S_0) and first A′ (π,π^*) singlet excited (S_1) electronic states. Second, dynamical calculations have been performed on the S_0 and S_1 potential energy surfaces to quantify the time scales of the process. The details of both sets of calculations follow.

2.1. Electronic-Structure Calculations. Two different electronic methodologies were employed in order to perform the exploration of the S_0 and S_1 states. First, optimizations with Hartree−Fock (HF) for S_0 and CIS[29] for S_1 were performed with the Gaussian 03 program,[30] mainly to compare the results to those previously published. Second, density functional theory (DFT) and time-dependent DFT (TD-DFT)[31] optimizations were performed for the S_0 and S_1 states, respectively. The three-parameter hybrid functional of Becke with the correlation functional of Lee, Yang, and Parr (B3LYP)[32,33] was chosen. Since the Gaussian suite of programs does not allow one to perform optimizations in the TD-DFT scheme, we made use of the TURBOMOLE program (version 5.6)[34,35] for such calculations. Complementary calculations with the complete active space self-consistent field (CASSCF) method[36] and the CASSCF at the second-order perturbation theory (CASPT2) energy point calculations, both with an active space of 12 electrons and 10 molecular orbitals of A″ symmetry, including all the π system, were carried out with the MOLCAS program (version 6.2)[37] to evaluate vertical excitation energies. For all cases, the 6-31G(d,p)[38,39] basis set was used.

The calculations necessary for building the potential energy surfaces for the S_0 and S_1 electronic states used in the dynamical simulations were performed with the Gaussian 03 program, as we verified that the results produced by the B3LYP functionals used in the Gaussian and TURBOMOLE packages differ by up to 0.04 kcal mol^{-1} in the relative stability of the stationary points we calculated. This small difference comes from the use of a different form of the local correlation functional. The Gaussian package uses the VWN(III) local correlation functional, whereas TURBOMOLE uses VWN(V).[40]

2.2. Nuclear Quantum Dynamical Calculations. Quantum dynamical calculations were carried out by means of wave-packet propagation on a three-dimensional reduced model of the S_0 and S_1 potential energy hypersurfaces. A time-dependent self-consistent field approximation was adopted.[41] In particular, the Heidelberg multiconfiguration time-dependent Hartree package (MCTDH)[42] was used. Recently, this method has successfully been applied in different aspects of multidimensional intramolecular proton-transfer systems.[43−45] A brief description of the method is presented here.

The MCTDH method is a general algorithm to solve the time-dependent Schrödinger equation. The MCTDH wave function is expanded in a sum of the products of so-called single-particle functions (SPFs). The SPFs $\varphi(\mathbf{q},t)$ may be one- or multidimensional functions, and, in this case, the coordinate $\mathbf{q}$ is a collective function, $\mathbf{q} = (Q_k, ..., Q_j)$. Because the SPFs are time-dependent, they follow the wave packet, and often a rather small number of SPFs suffices for convergence.

The ansatz for the MCTDH wave function reads

$$\Psi(Q_1, ..., Q_f, t) \equiv \Psi(q_1, ..., q_p, t) = \sum_{j_1}^{n_1}\cdots\sum_{j_p}^{n_p} A_{j1,...,jp}\prod_{\kappa=1}^{p}\varphi_{j_k}^{(\kappa)}(q_\kappa, t) \quad (1)$$

where f denotes the number of degrees of freedom, and p is the number of MCTDH particles, also called the combined modes. There are n_κ SPFs for the κth particle. The equations of motion for the coefficient vector $\mathbf{A}$ and for the SPFs are derived from a variational principle. It is important to note that MCTDH uses, in a variational sense, optimal SPFs, as this ensures the fastest convergence. The equations of motion are complicated, but because there are comparatively few equations to be solved, the MCTDH method can be very efficient.

The solution of the equations of motion requires that one builds the mean fields at every time step. The development of the constant mean-field integrator has reduced the number of mean-field evaluations by typically a factor of 10, but a fast evaluation of the mean fields is still essential. Such a fast algorithm exists if the Hamiltonian can be written as a sum of the products of monoparticle operators:

$$\hat{H} = \sum_{r=1}^{s} c_r \prod_{\kappa=1}^{p} \hat{h}_r^{(\kappa)} \quad (2)$$

where $\hat{h}_r^{(\kappa)}$ operates on the κth particle only, and c_r represents numbers. The Hamiltonian for this work will be designed to fit to this product form.

3. Results and Discussion

3.1. Electronic-Structure Calculations. *3.1.1. Ground Electronic State.* The exploration of the electronic ground state led to the optimization of five minima at all levels of calculation. These structures, which were previously characterized at the

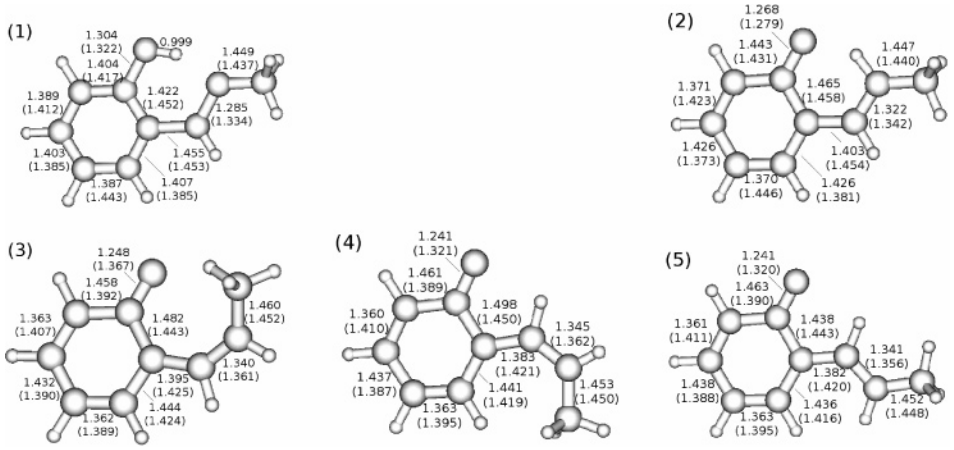

Figure 2. Optimized geometrical structures of the tautomers of the SMA molecule: (1) enol, (2) cis-keto, (3) trans-keto *a*, (4) trans-keto *b*, and (5) trans-keto *c*. Some distances in Å at the $S_0(S_1)$ states are given for the DFT(TD-DFT) levels. The values for the excited enol form were obtained after optimization of the ground electronic state enol geometry fixing the O−H distance at 0.999 Å.

TABLE 1: Ground Electronic State Relative Potential Energies (kcal mol^{-1}) of the Five Different Tautomers of the SMA and of the Transition State for the Proton Transfer (TS)

structure	HF	DFT
enol	0	0
cis-keto	8.40	5.00
trans-keto *a*	21.15	19.12
trans-keto *b*	18.32	18.49
trans-keto *c*	15.67	16.18
TS (enol → cis-keto)	14.81	5.90

HF/6-31G(d) level by Zgierski and Grabowska, are (in the same nomenclature employed in ref 25) the enol, the cis-keto and the three trans-keto (*a*, *b*, and *c*) tautomers (Figure 2).

Table 1 shows the relative potential energies of all optimized structures referred to the enol form (in kcal mol^{-1}). It is observed that the proton transfer in S_0 is an endoergic process at both levels of calculations.

Results obtained at the HF level agree with those previously published by Zgierski and Grabowska[25] with just small differences due to the slightly different basis set used. Of the five minima located, only the trans-keto *a* form does not possess a symmetry plane. The transition-state geometry of the proton transfer between the enol and the cis-keto forms was also located and characterized with an imaginary frequency of 1641*i* cm^{-1}, leading to an energy barrier of 14.81 kcal mol^{-1}.

DFT calculations agree with the HF results in assigning the relative stability of the five isomers of the SMA. A transition-state structure was also found with an imaginary frequency of 951*i* cm^{-1}, leading to a energy barrier of 5.90 kcal mol^{-1}. This value is not as high as the one calculated for the HF level of theory. In any case, the reverse energy barrier lays only 0.90 kcal mol^{-1} above the cis-keto minimum, which could hardly prevent the cis-keto form from reverting to the enol.

According to all these results, the net proton-transfer reaction cannot take place in the S_0 state.

3.1.2. First Singlet Excited Electronic State. As previously stated, one of the few experimental measurements published for the SMA in the S_1 state is the energy of the absorption maximum. We theoretically evaluated this energy at the different methods of calculation with single-point excitation calculations from the optimized enol structure in S_0. The results are displayed and compared to the experimental data in Table 2. As we have previously mentioned, CIS exaggerates the excitation energy. It can be seen that CASSCF and CASPT2 make a better prediction, whereas TD-DFT is closest to the experimental result.

TABLE 2: Calculated Vertical Excitation Energies (cm^{-1}) of the Optimized Enol Tautomer of SMA from the Ground Electronic State to the First (π,π^*) Singlet Excited Electronic State

CIS	45 278
CASSCF	33 940
CASPT2	35 346
TD-DFT	32 796
experimental value (ref 24)	∼32 000

TABLE 3: First Singlet Electronic State Relative Potential Energies (kcal mol^{-1}) of the Five Different Tautomers of the SMA and of the Transition State for the Proton Transfer (TS)

structure	CIS	TD-DFT
enol	16.14	
cis-keto	0	0
trans-keto *a*	9.28	5.09
trans-keto *b*	6.24	2.97
trans-keto *c*	2.92	−0.44
TS (enol → cis-keto)	17.32	

In Table 3, the relative stabilities of all the optimized structures in the S_1 potential surface related to the cis-keto form (in kcal mol^{-1}) is presented. In contrast to what has been observed in the exploration of the S_0 state, the proton transfer becomes exoergic, and the energy barrier decreases substantially in the S_1 state. The cis-keto tautomer becomes more stable than the enol form in both cases. At the TD-DFT level, the enol form could not even be located as a stable minimum, and the trans-keto *c* tautomer becomes the most stable structure at the TD-DFT level.

CIS calculations practically coincide with the data published by Zgierski and Grabowska.[25] We can observe that the proton-transfer reaction becomes largely exoergic, and that there is an important decrease in the energy barrier in comparison with the S_0 state, which is a first indication of the existence of an ESIPT.

TD-DFT results are quite different in the exploration of the S_1 state in comparison with the DFT exploration of S_0. All the attempts failed to locate a TD-DFT minimum in the enol region. This suggests a barrierless ESIPT process, which involves the absence of a transition-state structure. A set of relaxed reaction coordinate calculations was carried out varying the O−H distance and allowing the rest of the geometry to relax and attain minimum energy. The reaction profile obtained, depicted in

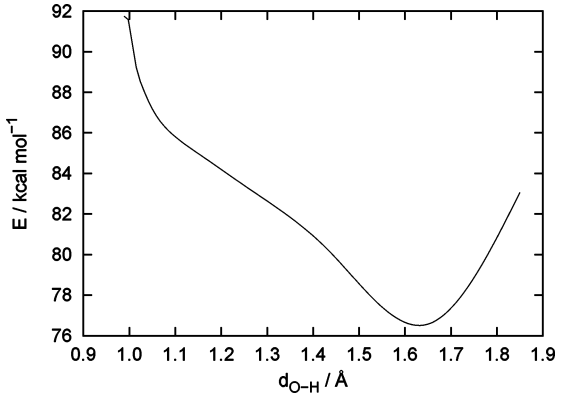

Figure 3. TD-DFT proton-transfer reaction profile relaxed along the O−H distance for the first (π,π^*) singlet excited electronic state. Energy origin is the energy of the DFT-optimized enol form in S_0.

Figure 3, confirms that the ESIPT is indeed barrierless at this level of theory.

Figure 2 also depicts the values for some relevant interatomic distances in all forms of the SMA at the DFT and TD-DFT levels. It is worth noting that the enol−cis-keto proton transfer in S_0 involves a substantial energy barrier because of the loss of aromaticity along the process. This effect is notably weaker in S_1 because the enol form has already lost a certain aromatic character in the excitation process. In effect, in the excited form of the enol tautomer, the C−C distances in the six-member ring present quite disparate values (the difference between the longest and shortest distances is equal to 0.067 Å), in comparison with S_0 (where this difference equals 0.035 Å), indicating a loss of aromaticity, which favors the ESIPT reaction.

As a conclusion of this electronic study of SMA, we believe that the DFT/TD-DFT methods provide, with a not-too-high cost of calculation, reasonably accurate results for the SMA system that are in good agreement with the experimental data published. Furthermore, it is accepted that the DFT/TD-DFT levels provide a good description for the excitation energy of valence excited (π,π^*) states.[46] This encouraged us to use this level of calculation in the building up of the S_0 and S_1 potential energy surfaces needed in our quantum dynamical calculations.

3.2. Nuclear Quantum Dynamical Calculations. To our knowledge, the dynamical study previously published for the ESIPT in SMA[25] was carried out with the approximate semiclassical instanton approach on CIS-quality electronic structure data. Because our results applying the DFT/TD-DFT methodology show us that the proton transfer is actually a barrierless process in S_1, we concluded that a quantum dynamics simulation with the energy origin at the vertical excitation would be more suitable for this system.

However, before studying any molecular system from the dynamical point of view, it is necessary to describe it properly by choosing a set of coordinates adapted to the physical representation of the reaction. This choice is a very important step in the dynamical study of any system because it will define the form of the molecular Hamiltonian operator.

Rigorous quantum dynamical study of a molecular system is a daunting task, even for small systems. In the time-dependent picture, part of the problem lies within the implicit difficulty in propagating a highly dimensional wave packet representing the state of the system. Highly efficient wave-packet propagation algorithms such as MCTDH[42] have eased this task, which, even though still far from being routine work, is now possible for systems of moderate size. A very serious limitation of this kind of study, however, resides in the adequate representation of the potential energy surface, which conditions the time evolution of the system.

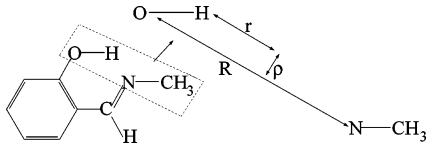

Figure 4. Definition of the three-dimensional set of coordinates model for the proton-transfer reaction in SMA.

Before starting the dynamical study of the intramolecular proton transfer in the excited state for SMA, it is worth remembering that the amount of experimental data about the subject is exiguous, which will hinder proper comparison of theoretical predictions and experimental findings. Previous studies have relied on the existence of a potential energy barrier in S_1, which does not seem to exist. Accordingly, the purpose of the dynamical simulation will be to establish a reasonable value for the rate of the process through the use of a reasonably accurate quantum dynamical simulation carried out on a portion of the potential energy surface relevant to the process computed at an appropriate level of computation. To this end, we will apply several approximations that will render the system in a simple enough form but allow meaningful results to be obtained.

In what follows, we describe the model we used for the dynamical simulation of the ESIPT in SMA. It seems to be a reasonable assumption to restrict the motion of the proton to the molecular plane, which also contains the donor and acceptor atoms. As dynamical coordinates to represent the system, we chose a set of three internal coordinates relevant for the intramolecular proton transfer: (i) the distance between the oxygen and nitrogen atoms (R), (ii) the distance between the position of the hydrogen atom and the mediatrix of the O−N segment (r), and (iii) the distance between the position of the hydrogen atom and the straight line linking the donor and acceptor atoms at any time (ρ). It has been known for a time that, besides the position of the transferring proton, the distance between the donor and acceptor atoms is of great importance and thus should be included in the simulation.[47,48] It must be noted that, within our description, the values of $r \leq 0.0$ Å determine the reactant region, while values of $r > 0$ approximately correspond to the product region. This set of coordinates is centered in the proton transfer region of the molecule, as graphically depicted in Figure 4.

Next, the potential energy surfaces for the S_0 and S_1 states in the form $\hat{V}(R,r,\rho)$ are needed. To obtain these, a simple structure generator program was coded, which generates a structure from a set of values R, r, and ρ as follows: We divide the SMA molecule into four fragments: the aromatic ring and the ancillary C−H atoms (fragment 1), the oxygen atom (fragment 2), the N−CH_3 group (fragment 3), and the proton (fragment 4). Taking as a starting point the structure of the potential energy minimum in S_0 of SMA, the program moves fragments 2 and 3 apart to a distance value R. In doing so, the internal structure of all fragments is kept rigid, and both the N−CH_3 group and the O atom are moved apart proportionally to the inverse ratio of their masses while the ring remains static. This choice brings about configurations that are chemically more acceptable than, for instance, keeping the oxygen atom statically bound to the ring and placing the changes in R on the displacement of fragment 3 alone. The proton is finally placed according to the values of r and ρ, and a point energy calculation is performed for this structure at the DFT and TD-DFT levels for S_0 and S_1, respectively, with the B3LYP functional and the 6-31G(d,p) basis set, using the Gaussian 03 package. A total of 720 points

were calculated, with 12 points for R (from +2.15 to +3.25 Å), 15 points for r (from +0.70 to −0.70 Å), and 4 points for ρ (+1.34, +0.84, +0.34, and −0.15 Å), with +0.34 Å being the value of ρ at the DFT-optimized enol structure at the S_0 surface. Few points were included in ρ in comparison with those in R and r, since we verified that the ρ coordinate does not vary substantially along the proton-transfer reaction in both the S_0 and the S_1 states. This set of coordinates allows the two-dimensional motion of the proton in the molecular plane, as well as the approach of the donor and acceptor atoms, which has been proved to be relevant in proton-transfer processes.[47,48] We note that, while the coordinate set resulting from this approach is a convenient one, the dynamical treatment is approximate because of the specific procedure followed to compute the potential energy surface, specifically because changing the distance between the donor and acceptor atoms also modifies other coordinates that have been kept outside the dynamical model (e.g., the distance between the oxygen atom and its binding site in the ring, or the distance between the nitrogen atom and the carbon atom bound to the ring).

To obtain the expression of the kinetic energy operator, we adopted the following procedure: First, according to the restriction of motion in a plane, we only need to assign two Cartesian coordinates for each fragment, which leads us to a set of six Cartesian coordinates. Second, we establish the mathematical relationships between these six Cartesian coordinates and our set of three coordinates R, r, and ρ. For this we need to consider three more coordinates, corresponding to the two Cartesian coordinates of the center of mass and the global rotational angle of the three fragments in the plane. Finally, after some algebraic manipulation employing the chain rule, the ∇^2 operator can be expressed in terms of our new set of coordinates. In the final expression, the second derivatives with respect to the center-of-mass Cartesian coordinates can be separated. Furthermore, introducing the additional approximation that the global rotation in the plane does not significantly affect the proton transfer process, we finally reach an expression of the Hamiltonian operator which only depends on R, r, and ρ:

$$\hat{H} = \hat{T} + \hat{V}(R,r,\rho) \tag{3}$$

where $\hat{T}$ is

$$\begin{aligned}\hat{T} = &-\frac{1}{2}\left(\frac{1}{m_{\mathrm{N-CH_3}}}+\frac{1}{m_{\mathrm{O-ring}}}\right)\frac{\partial^2}{\partial R^2} - \\ &\frac{1}{2}\left[\left(\frac{1}{m_{\mathrm{N-CH_3}}}+\frac{1}{m_{\mathrm{O-ring}}}\right)\left(\frac{1}{4}+\frac{\rho^2}{R^2}\right)+\frac{1}{m_{\mathrm{H}}}\right]\frac{\partial^2}{\partial r^2} - \\ &\frac{1}{2}\left[\left(\frac{1}{m_{\mathrm{N-CH_3}}}+\frac{1}{m_{\mathrm{O-ring}}}\right)\left(\frac{1}{4}+\frac{r^2}{R^2}\right)+\frac{r}{R}\left(\frac{1}{m_{\mathrm{N-CH_3}}}-\frac{1}{m_{\mathrm{O-ring}}}\right)+\right. \\ &\left.\frac{1}{m_{\mathrm{H}}}\right]\frac{\partial^2}{\partial \rho^2}+\frac{1}{2}\left(\frac{1}{m_{\mathrm{N-CH_3}}}-\frac{1}{m_{\mathrm{O-ring}}}\right)\frac{\partial}{\partial R}\frac{\partial}{\partial r}+ \\ &\left[\frac{r\rho}{R^2}\left(\frac{1}{m_{\mathrm{N-CH_3}}}+\frac{1}{m_{\mathrm{O-ring}}}\right)+\frac{\rho}{2R}\left(\frac{1}{m_{\mathrm{N-CH_3}}}-\frac{1}{m_{\mathrm{O-ring}}}\right)\right]\frac{\partial}{\partial r}\frac{\partial}{\partial \rho} - \\ &\frac{1}{2R}\left(\frac{1}{m_{\mathrm{N-CH_3}}}+\frac{1}{m_{\mathrm{O-ring}}}\right)\frac{\partial}{\partial R}+\frac{1}{2}\left[\frac{1}{R}\left(\frac{1}{m_{\mathrm{N-CH_3}}}-\frac{1}{m_{\mathrm{O-ring}}}\right)+\right. \\ &\left.\frac{r}{R^2}\left(\frac{1}{m_{\mathrm{N-CH_3}}}+\frac{1}{m_{\mathrm{O-ring}}}\right)\right]\frac{\partial}{\partial r}+\frac{\rho}{2R^2}\left(\frac{1}{m_{\mathrm{N-CH_3}}}+\frac{1}{m_{\mathrm{O-ring}}}\right)\frac{\partial}{\partial \rho}\end{aligned} \tag{4}$$

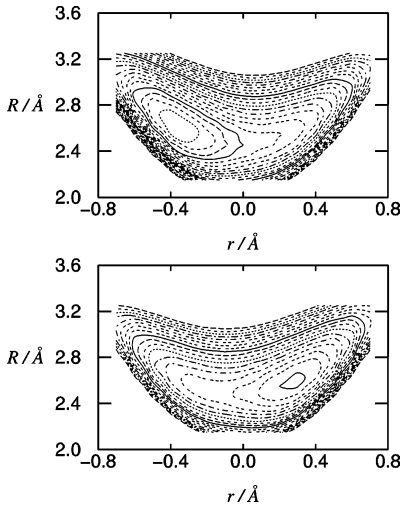

Figure 5. DFT/TD-DFT 6-31G(d,p) two-dimensional potential energy surface cuts (R, r, ρ = +0.34 Å) for the ground (top) and first singlet excited (bottom) electronic states of the SMA. The coordinates are explained in Figure 4.

where m_{H}, $m_{\mathrm{N-CH_3}}$, and $m_{\mathrm{O-ring}}$ denote the masses of the transferred proton (fragment 4), the N−CH_3 fragment (fragment 3), and the O−ring fragment (fragment 1 + fragment 2) of SMA, respectively. The resulting Hamiltonian is approximate: the kinetic energy term above assumes that the O atom and fragment 1 (the aromatic ring) do not move with respect to each other, while the potential energy surfaces have been constructed allowing such motion to chemically consider more significant structures. Because of this, the dynamical treatment is implicitly approximate, even within the three dimensions considered.

Figure 5 depicts the cuts of the S_0 and S_1 potential energy surfaces obtained (for ρ = +0.34 Å). Because each point of the grid was obtained by energy point calculations without allowing the molecule to relax and the actual value of ρ for the cis-keto minimum in S_0 is slightly different (+0.41 Å), the product energy minimum does not appear in this particular cut of S_0. Nevertheless, any dynamical calculation performed on S_0 requires a good description of the reactant region rather than that of the product. According to the values collected in Table 3, there is no reactant minimum in S_1 for the TD-DFT level of theory, which agrees with the absence of the reactant energy minimum in the S_1 cut. We also verified that no exit channels exist neither in S_0 nor in S_1, so no absorbing potentials were necessary.

The steps followed in the dynamical calculations with the MCTDH package were as follows: First, the mesh of points for S_0 and S_1 were fitted by means of the POTFIT program, which is included in the MCTDH package, into direct product form, as required in eq 2. The initial wave packet consisted of a Gaussian function, which was propagated in imaginary time (i.e., relaxed) on the S_0 potential energy surface to locate the ground vibrational state. Finally, the resulting wave function was promoted to the S_1 potential surface according to the Franck−Condon principle. All the dynamical calculations performed were verified to be converged with respect to the basis of both primitive and SPF functions. Figure 6 shows six snapshots of the two-dimensional probability density of the wave packet for the first 25 fs of propagation, in the plane formed by r and R, with ρ = +0.34 Å.

As can be seen, the head of the wave packet reaches the product area along the r coordinate within 10 fs. From that point on, because our model is closed and does not include the rest

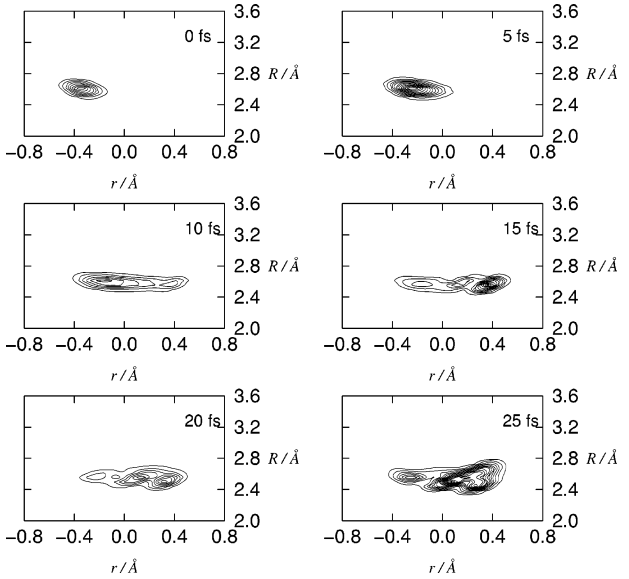

Figure 6. Snapshots of the (r, R, $\rho = +0.34$ Å) probability density for the three-dimensional simulation on the first excited electronic state at different times. The coordinates are explained in Figure 4.

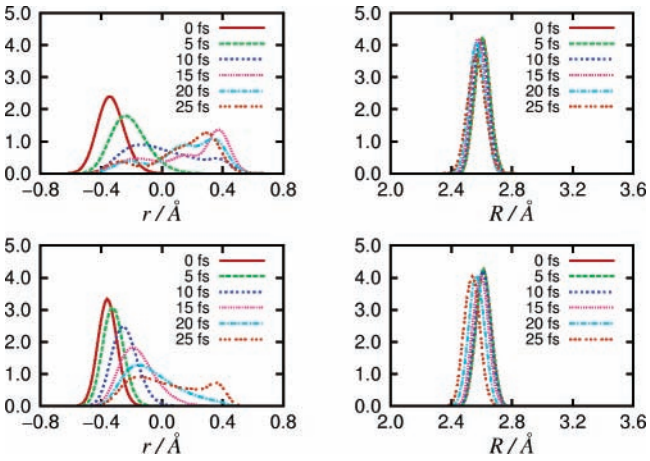

Figure 7. One-dimensional probability densities of the three-dimensional model at different times for r (left) and R (right) coordinates for the hydrogen (top) and deuterium (bottom) transfer. The coordinates are explained in Figure 4.

of vibrational modes, the propagated wave packet collides with the potential energy wall beyond the cis-keto region and consequently reflects. As a result, too many interference effects are observed. In addition to this, very little coupling with the R coordinate can be noticed, as the wave packet does not expand significantly along the R coordinate during the simulation time. If we plot the one-dimensional probability density for the r and R coordinates over time (Figure 7), it can be clearly seen how the wave packet propagates, collides, and comes back along the r coordinate in 25 fs, while the one-dimensional density of probability for the R coordinate does not vary substantially within the same time. The same behavior was observed for the ρ coordinate.

The isotopic substitution of the transferred proton for a deuterium was also studied. We compare in Figure 7 the one-dimensional probability densities for the r and R coordinates for the isotopic substituted system with the previous case. As expected, a slower evolution of the wave packet along the r coordinate is observed for the deuterated case, whereas, along the R coordinate, the wave packet moves further to shorter values than those in the nondeuterated case.

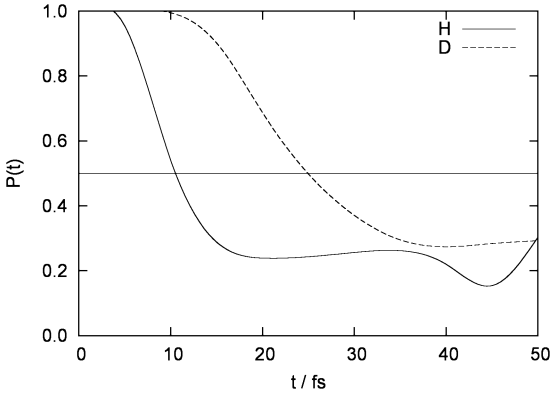

Figure 8. Survival probabilities for the hydrogen and deuterium transfers for the first 50 fs of propagation. The horizontal line sets the point where the 50% of the reactant turns into product.

To quantify the amount of remaining reactant during the proton-transfer reaction, we calculated the survival probability (eq 5) for the first 50 fs of propagation,

$$P(t) = \int \mathrm{d}\tau h_r(\tau)|\Psi(\tau)|^2 \qquad (5)$$

where $\mathrm{d}\tau$ is the volume element, and $h_r(\tau)$ is equal to 1 in the reactant region ($r \leq 0.0$ Å) and equal to 0 in the product region ($r > 0.0$ Å). Solving eq 5 is equivalent to integrating the one-dimensional probability density curves for $r \leq 0$. The results are depicted in Figure 8. It can be observed how the curve for the hydrogen transfer decreases much faster than that for the deuterium transfer. Within 11 fs, approximately 50% of the nondeuterated reactant has turned into product, whereas the deuterated SMA needs 25 fs to transform the same amount of reactant, so a strong kinetic isotope effect is observed.

As mentioned before, the dynamical model is approximate because it assumes that the oxygen atom does not move relative to the aromatic ring, while the potential energy surface has been constructed allowing this motion. This is necessary to scan relevant parts of the potential energy surface when constructing it. It would make less physical sense if increasing the value of R would only move the $N-CH_3$ fragment away, leaving the O atom at a fixed distance from the aromatic ring, but it represents an approximation beyond the reduction of the system to a three-dimensional model. From a chemical point of view, in such a fast process, keeping the internal structure of the aromatic ring frozen seems to be a reasonable approximation. However, rather than assuming that *both* the oxygen atom and the ring move solidarily, it seems more reasonable that the oxygen atom is the one that carries out most of the internal motion, while the aromatic ring remains static by virtue of its larger mass. A "correct" treatment in which this motion is considered is complex. It would require an increase in the number of dynamical parameters, making the potential energy evaluation much more expensive, and finally requiring a much more intricate kinetic energy term. Because of the large difference in mass between the oxygen atom and the aromatic ring, most of the motion will be experienced by the oxygen atom. A simple way to assess the sensitivity of the conclusions obtained so far would be to redo the dynamical calculations, but this time assuming that *only* the oxygen atom is moving. This can be estimated approximately by setting m_{O-ring} in eq 2 to simply m_O. If one does this, one sees that the hydrogen transfer process shows negligible changes, whereas for deuterium transfer, the transfer time increases slightly to 27 fs.

4. Conclusions

The proton-transfer dynamics in the aromatic Schiff base SMA has been theoretically analyzed by means of electronic-structure calculations at the HF and DFT levels of theory for the ground electronic state (S_0), and at the CIS and TD-DFT levels of theory for the first singlet excited electronic state (S_1), combined to quantum nuclear dynamics simulation. Complementary calculations at the CASSCF and CASPT2 levels have been carried out to determine vertical excitation energies. The SMA system presents five stable structural conformations in S_0: enol, cis-keto, and three different trans-keto tautomers. All of them are planar or almost planar. Our DFT electronic calculations show that the enol form is the most stable one. The proton-transfer reaction is endoergic, with an energy barrier of 5.9 kcal mol^{-1} and a reverse energy barrier of only 0.9 kcal mol^{-1}, which does not allow the net proton-transfer reaction to take place.

Upon the (π,π*) excitation of the enol form, a loss of aromaticity in the six-membered ring is observed, which destabilizes the structure and sets the cis-keto as the most stable tautomer in S_1. At the TD-DFT level of theory, the enol form does not correspond to a stable structure minimum, therefore only four minima could be located. In addition to this, the proton-transfer reaction becomes exoergic and barrierless. Finally, we highlight that the DFT/TD-DFT energy calculations and geometry optimizations have performed quite well in describing the photochemistry of SMA.

Two three-dimensional potential energy surfaces were fitted from a large set of electronic structure calculations for S_0 (DFT level of theory) and S_1 (TD-DFT level of theory). The time evolution of the wave packet was calculated with the MCTDH algorithm. Our quantum dynamical calculations predict a time scale of 11 and 25 fs for the hydrogen and deuterium transfers, respectively, in S_1. The process is somewhat faster than predicted by Zgierski and Grabowska (30 and 115 fs for the hydrogen and deuterium transfers, respectively).[25] This speed-up, especially for the deuterium case, can be explained if we take into account the barrierless nature of the process and the fact that the starting point of our dynamics was the Franck−Condon excitation energy of the enol form. However, taking into account that DFT tends to overestimate the strength of hydrogen bonds, and thus underestimate the energy barrier, it could be said that our measured rates are an upper limit for the rate of the studied process. Given that, as previously said, the CIS method overestimates the energy barriers, our results, together with the ones obtained by Zgierski and Grabowska,[25] fix the range of the actual rate of the excited-state proton transfer in SMA.

Finally, it must be remarked that, even when dealing with a barrierless process, a quantum dynamical treatment leads to a strong H/D kinetic isotope effect in S_1 for the enol−cis-keto proton transfer.

Acknowledgment. R.G. acknowledges the Spanish Ministerio de Educación y Ciencia for a Ramón y Cajal research contract. The authors are grateful for financial support from the Ministerio de Educación y Ciencia and the Fondo Europeo de Desarrollo Regional through project CTQ2005-07115/BQU, and from the DURSI de la Generalitat de Catalunya (2005SGR00400). Use of computational facilities at the Centre de Supercomputació de Catalunya is also acknowledged.

References and Notes

(1) Bouas-Laurent, H.; Durr, H. *Pure Appl. Chem.* **2001**, *73*, 639.
(2) Exelby, R.; Grinter, R. *Chem. Rev.* **1965**, *65*, 247.
(3) Senier, A.; Shepheard, F. G. *J. Chem. Soc.* **1909**, *95*, 1943.
(4) Barbara, P. F.; Rentzepis, P. M.; Brus, L. E. *J. Am. Chem. Soc.* **1980**, *102*, 2786.
(5) Vargas, V. *J. Phys. Chem. A* **2004**, *108*, 281.
(6) T. Rosenfeld, M. O.; Meyer, A. Y. *Mol. Photochem.* **1973**, *5*, 39.
(7) Knyazhansky, M. I.; Metelitsa, A. V.; Kletskii, M. E.; Millov, A. A.; Besugliy, S. *J. Mol. Struct.* **2000**, *526*, 65.
(8) Hadjoudis, E.; Mavridis, I. M. *Chem. Soc. Rev.* **2004**, *33*, 579.
(9) Zgierski, M. Z.; Grabowska, A. *J. Chem. Phys.* **2000**, *112*, 6329.
(10) Okabe, C.; Nakabayashi, T.; Inokuchi, Y.; Nishi, N.; Sekiya, H. *J. Chem. Phys.* **2004**, *121*, 9436.
(11) Mitra, S.; Tamai, N. *Chem. Phys.* **1999**, *246*, 463.
(12) Kownacki, K.; Mordzinski, A.; Wilbrandt, R.; Grabowska, A. *Chem. Phys. Lett.* **1994**, *277*, 270.
(13) Rawat, M. S. M.; Norula, J. L. *Indian J. Chem., Sect. B* **1987**, *26*, 232.
(14) Kawato, T.; Kanatomi, H.; Koyama, H.; Igarashi, T. *J. Photochem.* **1986**, *33*, 199.
(15) Sackmann, E. *J. Am. Chem. Soc.* **1971**, *93*, 7088.
(16) Rau, H.; Luddecke, E. *J. Am. Chem. Soc.* **1982**, *104*, 1616.
(17) Irie, M.; Mohri, M. *J. Org. Chem.* **1988**, *53*, 803.
(18) Yokoyama, Y. *Chem. Rev.* **2000**, *100*, 1717.
(19) Irie, M. *Chem. Rev.* **2000**, *100*, 1685.
(20) Benniston, A. C. *Chem. Soc. Rev.* **2004**, *33*, 573.
(21) Ziolek, M.; Kubicki, J.; Maciejewski, A.; Naskrecki, R.; Grabowska, A. *Phys. Chem. Chem. Phys.* **2004**, *6*, 4682.
(22) Goodson, L. H.; Christopher, H. *J. Am. Chem. Soc.* **1949**, *71*, 1117.
(23) Lee, H.; Kitagawa, T. *Bull. Chem. Soc. Jpn.* **1986**, *59*, 2897.
(24) Grabowska, A.; Kownacki, K.; Kaczmarek, L. *Acta Phys. Pol., A* **1995**, *88*, 1081.
(25) Zgierski, M. Z.; Grabowska, A. *J. Chem. Phys.* **2000**, *113*, 7845.
(26) Siebrand, W.; Smedarchina, Z.; Zgierski, M. Z.; Fernández-Ramos, A. *Int. Rev. Phys. Chem.* **1999**, *18*, 5.
(27) Scheiner, S. *J. Phys. Chem. A* **2000**, *104*, 5898.
(28) Vendrell, O.; Moreno, M.; Lluch, J. M. *J. Chem. Phys.* **2002**, *117*, 7525.
(29) Foresman, J. B.; Head-Gordon, M.; Pople, J. A.; Frisch, M. J. *J. Phys. Chem.* **1992**, *96*, 135.
(30) Frisch, M. J.; Trucks, G. W.; Schlegel, H. B.; Scuseria, G. E.; Robb, M. A.; Cheeseman, J. R.; Montgomery, J. A., Jr.; Vreven, T.; Kudin, K. N.; Burant, J. C.; Millam, J. M.; Iyengar, S. S.; Tomasi, J.; Barone, V.; Mennucci, B.; Cossi, M.; Scalmani, G.; Rega, N.; Petersson, G. A.; Nakatsuji, H.; Hada, M.; Ehara, M.; Toyota, K.; Fukuda, R.; Hasegawa, J.; Ishida, M.; Nakajima, T.; Honda, Y.; Kitao, O.; Nakai, H.; Klene, M.; Li, X.; Knox, J. E.; Hratchian, H. P.; Cross, J. B.; Bakken, V.; Adamo, C.; Jaramillo, J.; Gomperts, R.; Stratmann, R. E.; Yazyev, O.; Austin, A. J.; Cammi, R.; Pomelli, C.; Ochterski, J. W.; Ayala, P. Y.; Morokuma, K.; Voth, G. A.; Salvador, P.; Dannenberg, J. J.; Zakrzewski, V. G.; Dapprich, S.; Daniels, A. D.; Strain, M. C.; Farkas, O.; Malick, D. K.; Rabuck, A. D.; Raghavachari, K.; Foresman, J. B.; Ortiz, J. V.; Cui, Q.; Baboul, A. G.; Clifford, S.; Cioslowski, J.; Stefanov, B. B.; Liu, G.; Liashenko, A.; Piskorz, P.; Komaromi, I.; Martin, R. L.; Fox, D. J.; Keith, T.; Al-Laham, M. A.; Peng, C. Y.; Nanayakkara, A.; Challacombe, M.; Gill, P. M. W.; Johnson, B.; Chen, W.; Wong, M. W.; Gonzalez, C.; Pople, J. A. *Gaussian 03*, revision C.03; Gaussian, Inc.: Wallingford, CT, 2004.
(31) Bauernschmitt, R.; Ahlrichs, R. *Chem. Phys. Lett.* **1996**, *256*, 454.
(32) Becke, A. D. *J. Chem. Phys.* **1993**, *98*, 5648.
(33) Lee, C.; Yang, W.; Parr, R. *Phys. Rev. B* **1988**, *37*, 785.
(34) Furche, F.; Ahlrichs, R. *J. Chem. Phys.* **2002**, *117*, 7433.
(35) Ahlrichs, R.; Bär, M.; Hiäser, M.; Horn, H.; Kölmel, C. *Chem. Phys. Lett.* **1989**, *162*, 165.
(36) Anderson, K.; Malmqvist, P.-A.; Roos, B. O. *J. Chem. Phys.* **1992**, *96*, 1218.
(37) Andersson, K.; Barysz, M.; Bernhardsson, A.; Blomberg, M. R. A.; Carissan, Y.; Cooper, D. L.; Fülscher, M. P.; Gagliardi, L.; de Graaf, C.; Hess, B. A.; Hagberg, D.; Karlström, G.; Lindh, R.; Malmqvist, P.-Å.; Nakajima, T.; Neogrády, P.; Olsen, J.; Raab, J.; Roos, B. O.; Ryde, U.; Schimmelpfennig, B.; Schütz, M.; Seijo, L.; Serrano-Andrés, L.; Siegbahn, P. E. M.; Stålring, J.; Thorsteinsson, T.; Veryazov, V.; Widmark, P.-O. *MOLCAS*, version 6.2; Lund University: Lund, Sweden, 2000.
(38) Hariharan, P.; Pople, J. *Theor. Chim. Acta* **1973**, *28*, 213.
(39) Francl, M.; Petro, W.; Hehre, W.; Binkley, J.; Gordon, M.; DeFrees, D.; Pople, J. *J. Chem. Phys.* **1982**, *77*, 3654.
(40) Vosko, S. H.; Wilk, L.; Nusaic, M. *Can. J. Phys.* **1980**, *58*, 1200.
(41) Makri, N.; Miller, W. H. *J. Chem. Phys.* **1987**, *87*, 5781.
(42) Worth, G. A.; Beck, M. H.; Jäckle, A.; Meyer, H.-D. *The MCTDH Package*, version 8.2; Ruprecht-Karls-Universität Heidelberg, Heidelberg,

Germany, 2000. Meyer, H.-D. *The MCTDH Package*, version 8.3; Ruprecht-Karls-Universität Heidelberg, Heidelberg, Germany, 2002. See http://www.pci.uni-heidelberg.de/tc/usr/mctdh/.

(43) Naundorf, H.; Worth, G.; Meyer, H.-D.; Kühn, O. *J. Phys. Chem. A* **2002**, *106*, 719.

(44) Petković, M.; Kühn, O. *J. Phys. Chem. A* **2003**, *107*, 8458.

(45) Petković, M.; Kühn, O. *Chem. Phys.* **2004**, *304*, 91.

(46) Dierksen, M.; Grimme, S. *J. Phys. Chem. A* **2004**, *108*, 10225.

(47) Bosch, E.; Moreno, M.; Lluch, J. M.; Bertrán, J. *J. Chem. Phys.* **1990**, *93*, 5685.

(48) Paz, J. J.; Moreno, M.; Lluch, J. M. *J. Chem. Phys.* **1995**, *103*, 353.